

The mobility of dual vortices in honeycomb, square, triangular, Kagome and dice lattices

Longhua Jiang and Jinwu Ye

Physics Department, The Pennsylvania State University, University Park, PA, 16802

Abstract. It was known that by a duality transformation, interacting bosons at filling factor $f = p/q$ hopping on a lattice can be mapped to interacting vortices hopping on the dual lattice subject to a fluctuating dual "magnetic field" whose average strength through a dual plaquette is equal to the boson density $f = p/q$. So the kinetic term of the vortices is the same as the Hofstadter problem of electrons moving in a lattice in the presence of $f = p/q$ flux per plaquette. Motivated by this mapping, we study the Hofstadter bands of vortices hopping in the presence of magnetic flux $f = p/q$ per plaquette on five most common bipartite and frustrated lattices namely square, honeycomb, triangular, dice and Kagome lattices. We count the total number of bands, determine the number of minima and their locations in the lowest band. We also numerically calculate the bandwidths of the lowest Hofstadter bands in these lattices that directly measure the mobility of the dual vortices. The less mobile the dual vortices are, the more likely in a superfluid state the bosons are. We find that except the Kagome lattice at odd q , they all satisfy the exponential decay law $W = Ae^{-cq}$ even at the smallest q . At given q , the bandwidth W decreases in the order of Triangle, Square and Honeycomb lattice. This indicates that the domain of the superfluid state of the original bosons increases in the order of the corresponding direct lattices: Honeycomb, Square and Triangular. When $q = 2$, we find that the lowest Hofstadter band is completely flat for both Kagome and dice lattices. There is a gap on Kagome lattice, but no gap on dice lattice. This indicates that the boson ground state at half filling with nearest neighbor hopping on Kagome lattice is always a superfluid state. The superfluid state remains stable slightly away from the half filling. Our results show that the behaviours of bosons at or near half filling on Kagome lattice are quite distinct from those in square, honeycomb and triangular lattices studied previously.

1. Introduction

The Extended Boson Hubbard model with various kinds of interactions, at various kinds of lattices (bipartite or frustrated) at various kinds of filling factors (commensurate $f = p/q$ or incommensurate) is described by the following Hamiltonian [5, 6, 7]:

$$H = \sum_{\langle ij \rangle} t (\alpha_i^\dagger b_j + h.c.) + \sum_i n_i + \frac{U}{2} \sum_i n_i (n_i - 1) + V_1 \sum_{\langle ij \rangle} n_i n_j + V_2 \sum_{\langle\langle ik \rangle\rangle} n_i n_k + \quad (1)$$

where $n_i = b_i^\dagger b_i$ is the boson density and $U; V_1; V_2$ are onsite, nearest neighbor (nn) and next nearest neighbor (nnn) interactions between the bosons. The model may include further neighbor interactions and possible ring-exchange interactions. For a bipartite lattice, the sign of t can be changed by changing the sign of b_i in one of the two sublattices. But in a frustrated lattice, the sign of t makes a difference.

It is very important to extend Boson Hubbard model in bipartite lattices to frustrated lattices such as triangular, dice and Kagome lattices, because of the following motivations:

(1) For atom adsorptions on bare graphite, the preferred adsorption sites form a triangular lattice. The phase diagrams of coverage (the filling factor) versus temperature resulting from the competitions of these energy scales are very diverse and rich [1, 2]. It was believed that Eqn.1 may capture the main physics of the phenomena.

(2) Atomic physicists are trying to construct an effective two dimensional frustrated optical lattices using laser beams and then load either ultra-cold fermion or boson atoms at different filling factors on the lattice. They may tune the parameters to realize different phases by going through quantum phase transitions [3, 4].

(3) In the hard-core limit $U \rightarrow \infty$, due to the exact mapping between the boson operator and the spin $s = 1/2$ operator: $b_i^\dagger = S_i^+$; $b_i = S_i^-$; $n_i = S_i^z + 1/2$, the boson model Eqn.1 can be mapped to an anisotropic $S = 1/2$ quantum spin model in an external magnetic field [7, 6]:

$$H = \sum_{\langle ij \rangle} 2t (S_i^x S_j^x + S_i^y S_j^y) + V_1 \sum_{\langle ij \rangle} S_i^z S_j^z + V_2 \sum_{\langle\langle ik \rangle\rangle} S_i^z S_k^z + h \sum_i S_i^z + \quad (2)$$

where $h = -2V_1 - 2V_2$ for a square lattice. Note that in this Hamiltonian, there is a ferromagnetic coupling in the XY spin components and anti-ferromagnetic coupling in the Z spin component. Again, in a bipartite lattice, the sign of t can be changed by changing the sign of $S_i^x; S_i^y$ in one of the two sublattices, but keeping S_i^z untouched, so Eqn. 2 is the same as Quantum Heisenberg Antiferromagnet (QHA). However, in a frustrated lattice, the sign of t makes a difference, so Eqn. 2 is quite different from the QHA. The one to one correspondence between physical quantities in boson model and those in spin model are the boson density corresponds to the magnetization $n \rightarrow M$, the chemical potential corresponds to the magnetic field $\mu \rightarrow h$,

the compressibility corresponds to the susceptibility $\chi = \frac{\partial n}{\partial \mu} = \frac{\partial M}{\partial h}$. The boson number conservation corresponds to the $U(1)$ rotation around \hat{z} axis, the superfluid state $\langle b_i \rangle \neq 0$ corresponds to the XY ordered state $\langle S_i^+ \rangle \neq 0$, the charge ordered state corresponds to the modulation of $\langle S^z \rangle$. The supersolid corresponds to the simultaneous $\langle S_i^+ \rangle \neq 0$ and the modulation of $\langle S_i^z \rangle$ [6, 7]. In the hard-core limit, the Eqn.1 at half filling ($q = 2$) has the Particle-Hole (P-H) symmetry $b_i \leftrightarrow b_i^\dagger; n_i \leftrightarrow 1 - n_i$, it can be mapped to Eqn.2 in zero magnetic field $h = 0$ with the Time-reversal symmetry $S_i^+ \leftrightarrow S_i^-; S_i^z \leftrightarrow S_i^z$. Eqn.1 on triangular lattice at $q = 2$ is the prototype model to study supersolid state with P-H symmetry [7].

The model Eqn.1 with only the onsite interaction on square lattice was first studied in Ref.[5]. The effects of long range Coulomb interactions on the transition was studied in [8]. Very recently, the most general cases in square lattice at generic commensurate filling factors $f = p/q$ (p, q are relative prime numbers) were systematically studied in [9]. After performing the charge-vortex duality transformation [13], the authors in [9] obtained a dual theory of Eqn.1 in terms of the interacting vortices hopping on the dual lattice subject to a fluctuating dual "magnetic field". The average strength of the dual "magnetic field" through a dual plaquette is equal to the boson density $f = p/q$. This is similar to the Hofstadter problem of electrons moving in a crystal lattice in the presence of a magnetic field [10]. The magnetic space group (MSG) in the presence of this dual magnetic field dictates that there are at least q -fold degenerate minima in the mean field energy spectrum. The q minima can be labeled as $\phi_l; l = 0; 1; \dots; q-1$ which forms a q -dimensional representation of the MSG. In the continuum limit, the renormalized effective theory describing the superconductor to the insulator transition in terms of these q order parameters should be invariant under this MSG. If $\langle \phi_l \rangle = 0$ for every $l = 0, \dots, q-1$, the system is in the superfluid state. If $\langle \phi_l \rangle \neq 0$ for at least one l , the system is in the insulating state. In the supersolid state [6, 7, 12], one condenses a vortex-antivortex pair, but still keeps $\langle \phi_l \rangle = 0$ for every l . In the insulating or supersolid state, there must exist some kinds of charge density wave (CDW) (we assume that every boson carries one internal charge) or valence bond solid (VBS) states which may be stabilized by longer range interactions or possible ring exchange interactions included in Eqn.1. Very recently, the dual method was used to study the Extended Boson Hubbard model on a triangular lattice [11].

In a recent paper [12], one of the authors applied the dual approach of the extended boson Hubbard model Eqn.1 to study the reentrant "superfluid" in a narrow region of coverages in the second layer of ^4He adsorbed on graphite detected by Crowell and Reppy's torsional oscillator experiment in 1993 [15, 16]. He showed that there are two consecutive transitions at zero temperature driven by the coverage: a Commensurate-Charge Density Wave (CDW) at half filling to a narrow window of supersolid, then to an Incommensurate-CDW. In the Ising limit, the supersolid is a CDW supersolid; whereas in the easy-plane limit, it is a valence bond supersolid. Both transitions are second order transition with exact critical exponents $z = 2; \nu = 1/2; \beta = 0$. The results concluded that ^4He lattice supersolid was already observed in 1993. He also applied the same

dual method to study H_2/Kr /graphite system investigated in the recent experiment [14] and proposed that a judicious choice of substrate could also lead to an occurrence of hydrogen lattice supersolid. Implications to the realizations of a lattice supersolid of ultra-cold atoms in optical lattices were also given in Ref. [12].

Note that in the dual vortex picture, there are always interactions between vortices. Because the phase factors from the dual magnetic field only appear in the kinetic term, the interactions always commute with any generators in the MSG, so will not change the symmetry of the MSG.

In this paper, we study the Hofstadter bands of vortices hopping in the presence of dual magnetic field $f = p/q$ on the 5 most common bipartite and frustrated lattices such as square, honeycomb, triangular, dice and Kagome lattices. We especially study the bandwidth of the lowest bands. There are at least two motivations to study the bandwidth of the lowest bands (1) As pointed out in [9], as q becomes too large, the dual vortex method suffer the following two drawbacks (a) As dictated by the MSG, there are q minima in the BZ, so the distance in momentum space between these minima scales as $1/q$, the continuum theory only works at $k \ll 1/q$, therefore applies only at distance $\ll q$. The validity regime of the dual vortex theory shrinks. (b) When integrating out the vortex modes away from the minima, one encounters energy denominators determined by this bandwidth, so the dual vortex method may completely break down if the bandwidth becomes too small. By a simple argument, they estimated that at large q , the bandwidth W of the lowest Hofstadter band scales as $W \propto e^{-cq}$ with c at the order of 1 [18]. So the smaller the bandwidth, the smaller the valid regime of the dual vortex approach. (2) In the dual vortex picture, there are both a kinetic energy term and interactions between vortices. The kinetic term favors the moving of the vortices, while the interactions favor the localization of the vortices, the competition of the two energy scales may result all kinds of phases such as superfluid, CDW, VBS and even supersolid phase [12]. In this paper, we focus on the kinetic term only. Calculating the bandwidth of the kinetic term is very important, because the smaller of the bandwidth, the more inert the vortices (the less mobile the vortices are), therefore the boson superfluid state is more likely to occur.

By choosing suitable gauges and solve corresponding Harper's equations in the 5 lattices. we count the number of bands, determine the number of minima and their locations in the lowest Hofstadter bands. The results are listed in Table 1. We also numerically calculate the bandwidths of the lowest bands in these lattices at any q and test against the estimate $W \propto A e^{-cq}$. We believe that although the argument in [9] seems reasonable, it is far from being convincing. So it is important to test this argument by quantitative numerical calculations. We find that except the Kagome lattice at odd q , the exponential law is indeed satisfied and determine $(A; c)$ for the 5 different lattices. The results are listed in Table 2. We find that at given q , the bandwidth W decreases in the order of Triangle, Square and Honeycomb lattice. The corresponding direct lattices are honeycomb, square and triangular lattices, so the tendency to form a superfluid state increases. As shown in the Table 2, when $q = 2$, the lowest bands in both Dice

and Kagome lattices are flat. In dice lattice, the gap between the second flat band and the lowest flat band is $\frac{p}{6}$. It indicates that for the original boson at half filling with nearest neighbor hopping on the Kagome lattice, there could be only superfluid state. However, in Kagome lattice, the gap between the second dispersive band and the lowest flat band vanishes at $\mathbf{k} = (0;0)$, so the second dispersive band can not be ignored even in the lowest energy limit. Due to the gap vanishing on the Kagome lattice, we can not say definite things about the ground state in the original boson on a Dice lattice. There are some previous results on the energy spectra on square, honeycomb and triangular lattices [9, 9, 12, 11, 17] with different focuses. Our results on dual Dice and Kagome lattices, especially the discussions on the possible boson ground states on corresponding direct lattices are new and most interesting.

There are two equivalent methods to be used to study the Hofstadter bands. One is the Magnetic Brillouin Zone (MBZ) method to be employed in the main text. This method is physically more transparent and intuitive. Another is the symmetric method used in [9] and to be used in the appendix. This method treats x and y coordinates on equal footing, so is more symmetric than the first one. In the main text, we will use the first method to derive Harper's equations in the 5 lattices and then solve the equations analytically at small q and numerically at large q . In the appendix, we will use the second method to repeat the calculations. Although the coefficients of Harper's equations in the two schemes are different, as expected, we find that they result in the same energy spectra.

In the following, we will first study two bipartite lattices, namely square and honeycomb lattices, then we will investigate 3 frustrated lattices namely triangular, Dice and Kagome lattices. In the final section, we summarize our results in Table 1 and Table 2, we also comment on the results on CDW formations in high temperature superconductors claimed in [9] where q as large as 8;16;32 are used. In most of the cases, we focus on $p = 1$ case.

2. Square lattice

We are looking at the Hofstadter band of vortices hopping around square lattice in the presence of magnetic flux $\phi = p/q$ per square [9] (Fig.1). In the MBZ method, one

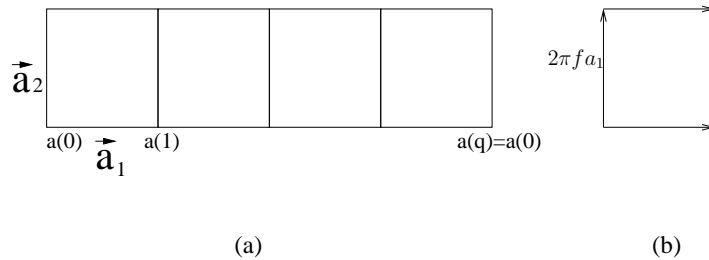


Fig 1: (a) a magnetic unit cell of square lattice, (b) Phase factors on bonds, 0 phase factors are not shown.

The mobility of dual vortices in honeycomb, square, triangular, Kagome and dice lattices 6

magnetic unit cell is q times larger than the conventional unit cell (Fig.1a). For the simplest gauge chosen in Fig.1(b), the hopping Hamiltonian is:

$$H = \sum_{\langle \mathbf{x}, \mathbf{y} \rangle} t_{\mathbf{x}, \mathbf{y}} [\psi_{\mathbf{x}} + a_1 > \langle \mathbf{x}, \mathbf{y} \rangle + \psi_{\mathbf{y}} + a_2 > e^{i2\pi \mathbf{f} a_1} \langle \mathbf{x}, \mathbf{y} \rangle + h.c.] \quad (3)$$

In the following, for simplicity, we set $t = 1$. The eigenvalue equation $H(\mathbf{k}) = E(\mathbf{k}) \psi(\mathbf{k})$ leads to the Harper's equation:

$$e^{ik_x} \psi_{l+1}(\mathbf{k}) - 2 \cos(2\pi \mathbf{f} l + k_y) \psi_l(\mathbf{k}) - e^{-ik_x} \psi_{l-1}(\mathbf{k}) = E(\mathbf{k}) \psi_l(\mathbf{k}) \quad (4)$$

where $l = 0; \dots; q-1; k_x = \frac{2\pi}{q} k; k_y = \frac{2\pi}{q} k$.

For small values of q , Eqn.4 can be solved analytically. For large values of q , we solve it numerically. There are always q bands. We focus on the lowest energy band and its bandwidth. As shown in [9], there are q minima at $(0; 2\pi \mathbf{f} l); l = 0; \dots; q-1$. The spectrum for $q = 4$ is shown in Fig. 2. In order to see clearly all the 4 MSG related minima, only part of the energy band close to the 4 minima in the lowest band is included. We also numerically calculated the bandwidth of the lowest band

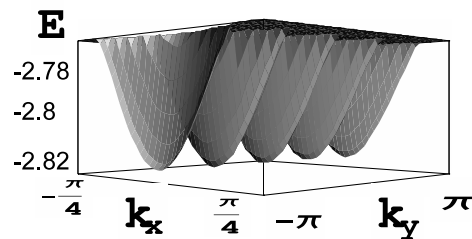


Fig 2: The lowest energy band of square lattice at $q = 4$.

upto $q = 18$. We found that it indeed satisfy the exponential law $W = A e^{-cq}$ with $A = 26.05; c = 1.20$. In a semi-log plot, it is a straight line which is shown in Fig.3

What is surprising is that even for the smallest $q = 1$ which is the non magnetic field case, the exponential law is still satisfied.

3. Honeycomb lattice

Honeycomb lattice is not a Bravais lattice, it can be thought as a underlying parallelogram Bravais lattice with two primitive vectors $\mathbf{a}_1 = \hat{x}; \mathbf{a}_2 = \frac{1}{2}\hat{x} + \frac{\sqrt{3}}{2}\hat{y}$ plus a two point basis located at $\mathbf{x} + \tilde{\mathbf{r}}$ and $\mathbf{x} + 2\tilde{\mathbf{r}}$ where $\tilde{\mathbf{r}} = \frac{1}{3}(\mathbf{a}_1 + \mathbf{a}_2)$ (Fig.2). Its

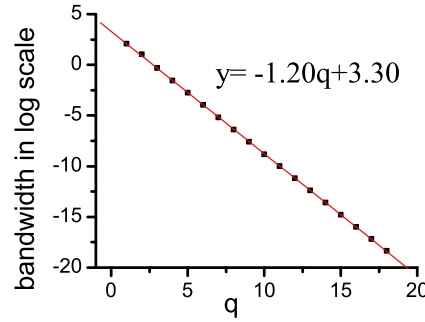


Fig 3: The bandwidth of lowest band in square lattice vs q

reciprocal lattice is also a parallelogram Bravais lattice spanned by $\vec{k} = k_1\vec{b}_1 + k_2\vec{b}_2$ with $\vec{b}_i = \frac{2\pi}{a_i} \hat{e}_{ij}$.

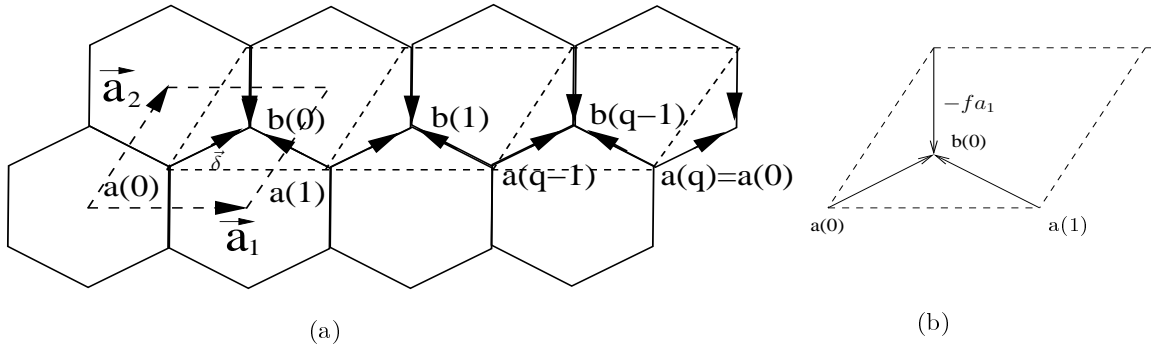


Fig 4: (a) A magnetic unit cell of honeycomb lattice (b) Phase factors on bonds, 0 phase factors are not shown

In the M B Z method, one magnetic unit cell is q times larger than the conventional unit cell (Fig.4a). In one conventional unit cell, there are also two atoms which are labeled by two color indices a and b (Fig.4). We are looking at the Hofstadter band of vortices hopping around a honeycomb lattice in the presence of magnetic flux $f = p/q$ per hexagon. For the simplest gauge chosen in Fig. 4(b), the vortex hopping Hamiltonian is:

$$H = \sum_{\vec{x}} \left[\sum_{\vec{j}} \left[\left| \vec{x} + \vec{\sim} \right\rangle \langle \vec{x} + \vec{j} | + \left| \vec{x} + \vec{\sim} \right\rangle \langle \vec{x} + \vec{a}_1 | \right. \right. \\ \left. \left. + \left| \vec{x} + \vec{\sim} \right\rangle \langle \vec{x} + \vec{a}_2 | + \text{h.c.} \right] \right] e^{i2\pi f \vec{a}_1 \cdot \vec{a}_2} \quad (5)$$

The Harper's equation is:

$$\begin{aligned} (1 + e^{i(k_x + 2\pi f l)}) \frac{a}{l}(\vec{k}) - e^{ik_y} \frac{a}{l+1}(\vec{k}) &= E(\vec{k}) \frac{b}{l}(\vec{k}) \\ (1 + e^{i(k_x + 2\pi f l)}) \frac{b}{l}(\vec{k}) - e^{ik_y} \frac{b}{l+1}(\vec{k}) &= E(\vec{k}) \frac{a}{l}(\vec{k}) \end{aligned} \quad (6)$$

where $l = 0; \dots, q-1$ is the flavor indices and a, b is the color indices, $k_x = \frac{2\pi}{a} x$.

For small values of q , Eqn.6 can be solved analytically. When $q = 1$, there is actually no magnetic field, it is just ordinary tight-binding model. There are

The mobility of dual vortices in honeycomb, square, triangular, Kagome and dice lattices [8]

two bands: $E(\mathbf{k}) = \frac{q}{3 + 2(\cos k_x + \cos k_y + \cos(k_x + k_y))}$. The lowest energy band is $E(\mathbf{k}) = \frac{q}{3 + 2(\cos k_x + \cos k_y + \cos(k_x + k_y))}$. There is only one minimum at $(0;0)$. The bandwidth is 3. The $q = 2$ case is especially interesting, because the original boson model can be mapped to a quantum $s = 1/2$ spin model [Eqn. 2] in a triangular lattice at zero field. For $q = 2$, there are 4 bands $E(\mathbf{k}) = \frac{q}{3 + 2A(\mathbf{k})}$ where $A(\mathbf{k}) = \frac{1}{2}(\cos 2k_1 + \cos 2k_2 - \cos(2k_1 - 2k_2))$. The lowest subband is $E(\mathbf{k}) = \frac{q}{3 + 2A(\mathbf{k})}$. There are 4 minima at $(\pm\pi; \pm\pi)$ and $(\pm\pi; 0)$ and $(0; \pm\pi)$. The 4 minima transform to each other under the MSG.

For general q , there are always $2q$ bands. As shown in [11, 17], there are two cases (1) q is odd, there are q minima at $(0; 2\pi/l); l = 0; \dots; q-1$. (2) q is even, there are $2q$ minima at $(\frac{2\pi}{3q}; \frac{2\pi}{3q} + 2\pi/l)$ where $l = 0; \dots; q-1$.

For large values of q , we solve Eqn. 6 numerically. Just like in square lattice, we focus on the energy band near the minima in the lowest energy band. The $q = 3$ and $q = 4$ spectrum are shown in Fig. 5(a), 5(b) respectively.

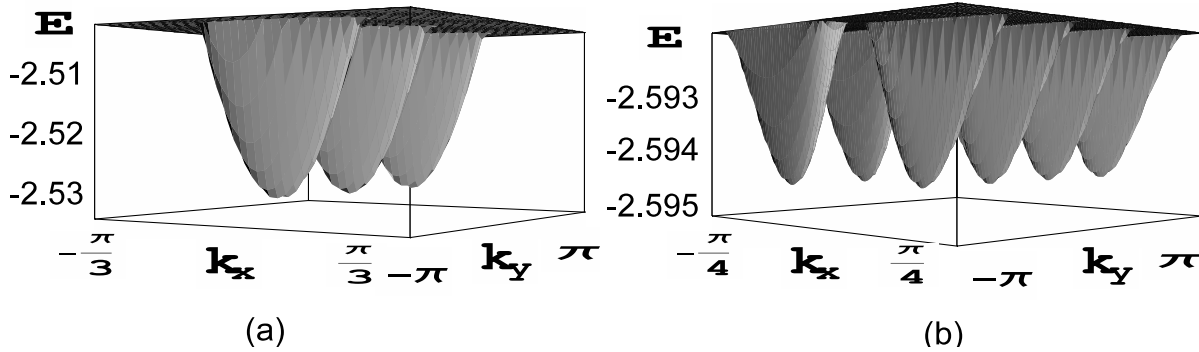


Fig 5: The lowest energy bands of honeycomb lattice at (a) $q = 3$, (b) $q = 4$

We also numerically calculated the bandwidths of the lowest band upto $q = 18$. We found that they satisfy the exponential law $W = Ae^{-cq}$ with $A = 11.82; c = 1.66$ for both q even and odd. In a semi-log plot, it is a straight line which is shown in Fig. 6.

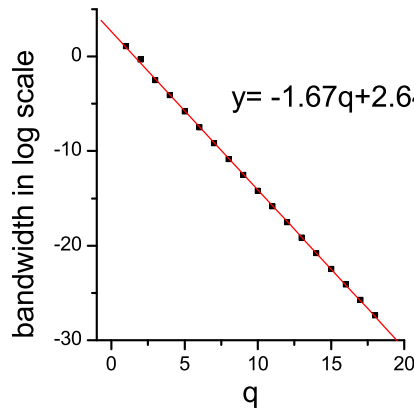


Fig 6: The bandwidth of honeycomb lattice vs q

What is surprising is that even for the smallest $q = 1$ which is the non-magnetic case, the exponential law is still satisfied.

4. Triangular lattice

In the previous two sections, we studied two bipartite lattices. In this section, we study the simplest frustrated lattice which is the triangular lattice. As said in the introduction, the physics in frustrated lattices could be very different from that in bipartite lattices.

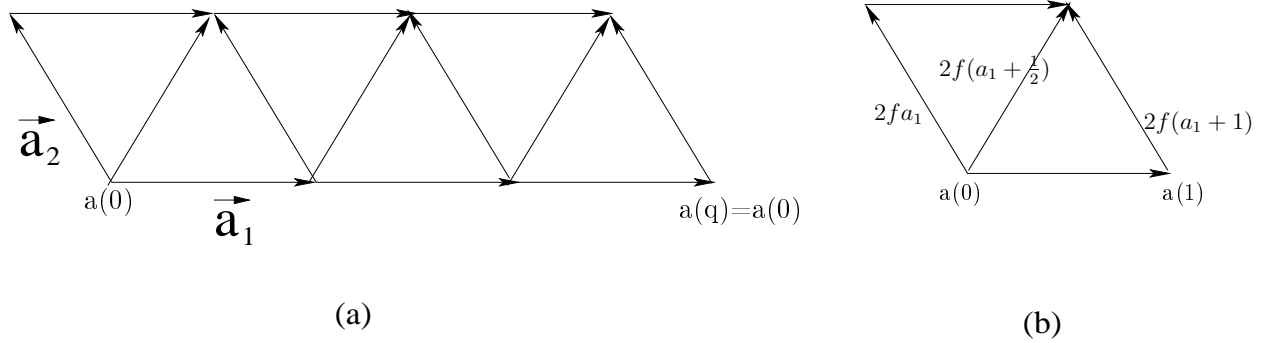


Fig 7: Triangular Lattice (a) magnetic unit cell of Triangular lattice, (b) Phase factors on bonds, 0 phase factors are not shown.

We are looking at the Hofstadter band of vortices hopping around a triangular lattice in the presence of magnetic flux $f = p/q$ per triangle. For the simplest gauge chosen in Fig. 7b, the Hamiltonian is:

$$H = \sum_{\mathbf{x}} [\mathbf{x} + \mathbf{a}_1 > \mathbf{x} \mathbf{j} + \mathbf{x} + \mathbf{a}_2 > e^{i2\pi f \mathbf{a}_1} < \mathbf{x} \mathbf{j} + \mathbf{x} + \mathbf{a}_1 + \mathbf{a}_2 > e^{i2\pi f (\mathbf{a}_1 + \frac{1}{2})} < \mathbf{x} \mathbf{j} + \mathbf{x} \mathbf{j}] \quad (7)$$

The corresponding Harper's equation is:

$$2 \cos(k_y + 2\pi f l) \psi_l(\mathbf{k}) = (e^{ik_x} + e^{i(k_x + k_y + 2\pi f (2l+1))}) \psi_{l+1}(\mathbf{k}) \\ (e^{ik_x} + e^{i(k_x + k_y + 2\pi f (2l+1))}) \psi_{l-1}(\mathbf{k}) = E(\mathbf{k}) \psi_l(\mathbf{k}) \quad (8)$$

where $l = 0; \dots; q-1$.

From the phase factors on the bond, it is easy to see that when q is even, there are only $\frac{q}{2}$ unit cells in one magnetic unit cell. Since the magnetic unit cell shrink to $\frac{q}{2}$, the range of k_x in the momentum space double its range accordingly. Therefore in Eqn.8, for q is odd, $\frac{2}{q} k_x \rightarrow \frac{2}{q}$, while for q even, $\frac{2}{q} k_x \rightarrow \frac{2}{q}$.

In fact, as shown in [9], there are three cases in a triangular lattice: (1) When q is odd, there are q bands. There are q minima at $(0; 4\pi f l); l = 0; \dots; q-1$ in the lowest band. (2) When q is even, there are $q/2$ bands. There are still two subcases: (2a). $q = 2n$ with n odd, there are $q/2$ minima at $(\frac{2}{3q}; \frac{2}{3q} + 4\pi f l), l = 0; \dots; \frac{q}{2}-1$. (2b). $q = 2n$ with n even, there are $\frac{q}{2}$ minima at $(0; 4\pi f l); l = 0; \dots; \frac{q}{2}-1$.

For $q = 1$ which is the non-magnetic case, the energy spectrum is $E(\mathbf{k}) = 2(\cos k_x + \cos k_y + \cos(k_x + k_y))$, there is only one minimum at $(0; 0)$. For $q = 2$, as

The mobility of dual vortices in honeycomb, square, triangular, Kagome and dice lattices 10

shown in [12], the spectrum is $E(\mathbf{k}) = -2(\cos k_x + \cos k_y + \cos(k_x + k_y))$. There are two minima located at $(-\frac{\pi}{3}; -\frac{\pi}{3})$

For large q , we solve Eqn.8 numerically. The results for $q = 3$ (odd case), $q = 6$ ($2n$ with n odd case) and $q = 8$ ($2n$ with n even case) are shown in Fig. 8a,b,c respectively.

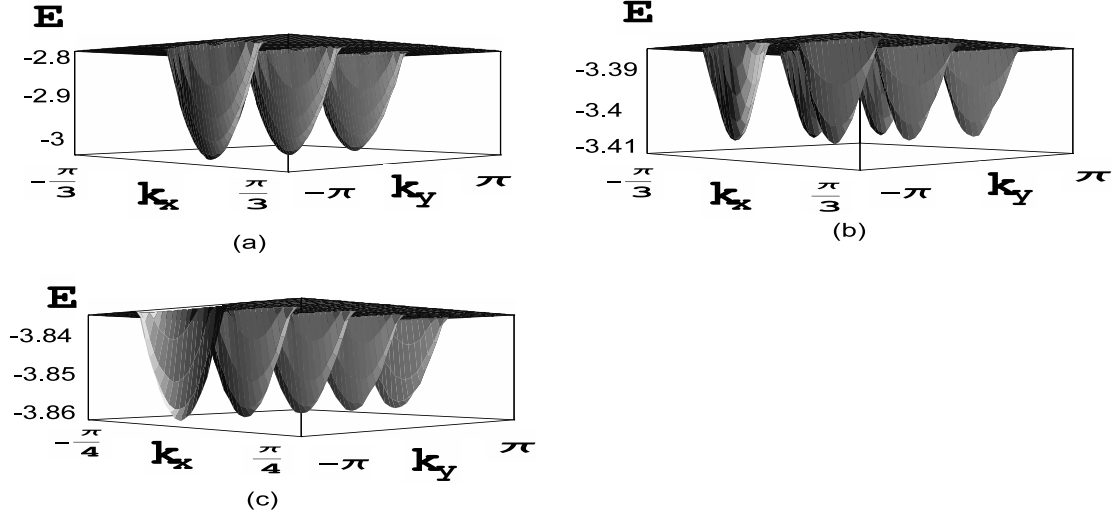


Fig 8: The lowest energy bands of triangular lattice at (a) $q = 3$, (b) $q = 6$, (c) $q = 8$

We also numerically calculated the bandwidth of the lowest band upto $q = 25$ for q is odd and upto $q = 30$ for q is even. For q odd, we find $A = 9.21; c = 0.82$ (Fig. 9a). For $q = 2n$, both n is odd and even, the bandwidth satisfy the same exponential law with $A = 55.70; c = 0.83$ (Fig.9b).

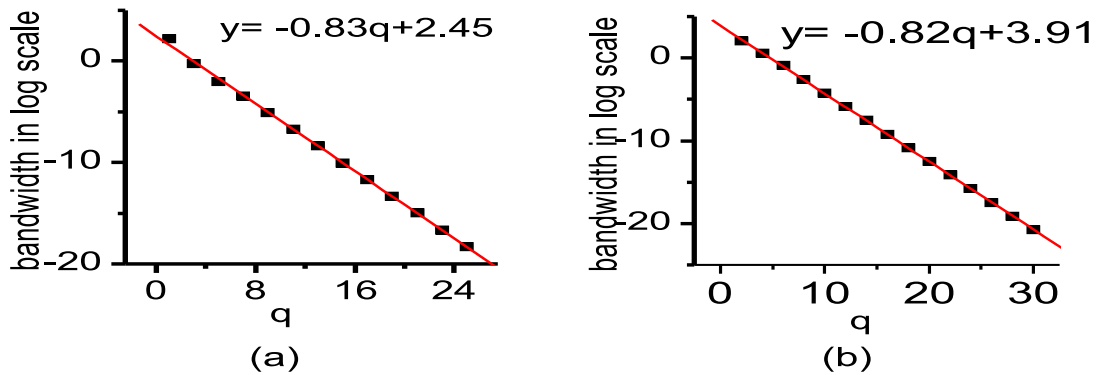


Fig 9: The bandwidth of triangular lattice vs q (a) q is odd, (b) q is even

5. Dice lattice

The dice lattice is the dual lattice of the Kagome lattice. It can be thought of consisting of two interpenetrating honeycomb lattice. Obviously, the dice lattice is not a Bravais lattice, it can be thought as a underlying parallelogram Bravais lattice with two primitive lattice vectors $\mathbf{a}_1 = \hat{x}$; $\mathbf{a}_2 = \frac{1}{2}\hat{x} + \frac{\sqrt{3}}{2}\hat{y}$ plus a three point basis labeled $a; b; c$ located at $\mathbf{x}; \mathbf{x} + \tilde{\mathbf{r}}; \mathbf{x} + 2\tilde{\mathbf{r}}$ where $\tilde{\mathbf{r}} = \frac{1}{3}(\mathbf{a}_1 + \mathbf{a}_2)$ (Fig.10). In contrast to the honeycomb lattice shown in Fig.4, the dice lattice is not a bipartite lattice and has a 3-sublattice structure.

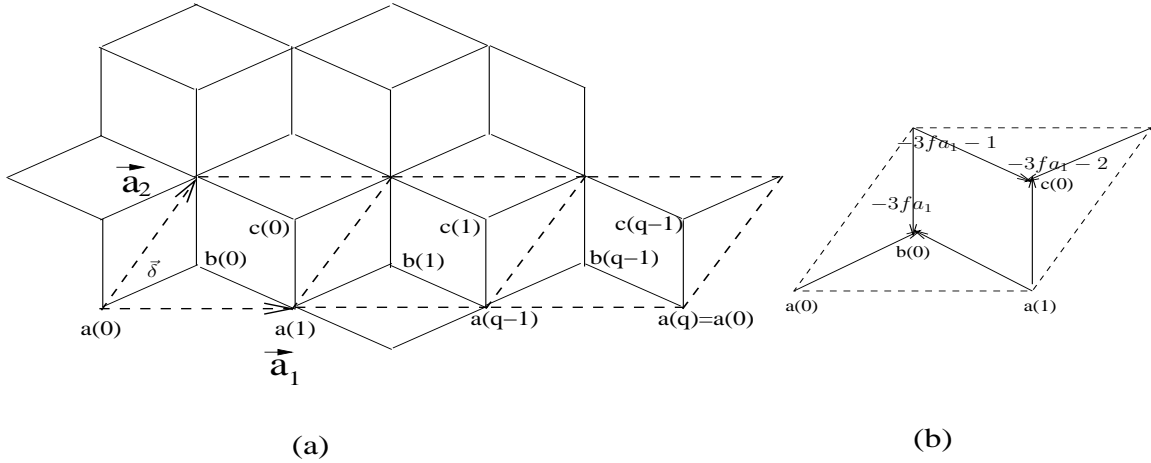


Fig 10: Dice Lattice (a) magnetic unit cell of Dice lattice, (b) Phase factors on bonds, 0 phase factors are not shown.

We are looking at the Hofstadter band of vortices hopping around a dice lattice in the presence of magnetic flux $\phi = p/q$ per parallelogram. For the simplest gauge chosen in Fig 10b, the Hamiltonian is:

$$\begin{aligned}
 H = & \sum_{\mathbf{x}} [\mathbf{j} + \tilde{\mathbf{r}} \rangle \langle \mathbf{x} | \mathbf{j} + \tilde{\mathbf{r}} \rangle e^{i2\pi f a_1} \langle \mathbf{x} + \mathbf{a}_2 | \mathbf{j} + \tilde{\mathbf{r}} \rangle \langle \mathbf{x} + \mathbf{a}_1 | \mathbf{j} \\
 & + \mathbf{j} + 2\tilde{\mathbf{r}} \rangle e^{i2\pi f(a_1 + \frac{1}{3})} \langle \mathbf{x} + \mathbf{a}_2 | \mathbf{j} + 2\tilde{\mathbf{r}} \rangle \langle \mathbf{x} + \mathbf{a}_1 | \mathbf{j} \\
 & + \mathbf{j} + 2\tilde{\mathbf{r}} \rangle e^{i2\pi f(a_1 + \frac{2}{3})} \langle \mathbf{x} + \mathbf{a}_1 + \mathbf{a}_2 | \mathbf{j} + 2\tilde{\mathbf{r}} \rangle] \quad (9)
 \end{aligned}$$

The corresponding Harper's equation is

$$\begin{aligned}
 (1 + e^{i(k_y + 2\pi f l)}) \hat{b}_l(\mathbf{k}) - e^{ik_x} \hat{b}_{l+1}(\mathbf{k}) - e^{i(k_y + 2\pi f(l + \frac{1}{3}))} \hat{c}_l(\mathbf{k}) \\
 (e^{ik_x} + e^{i(k_x + k_y + 2\pi f(l + \frac{2}{3}))}) \hat{c}_{l+1}(\mathbf{k}) = E(\mathbf{k}) \hat{a}_l(\mathbf{k}); \\
 (1 + e^{i(k_y + 2\pi f l)}) \hat{a}_l(\mathbf{k}) - e^{ik_x} \hat{a}_{l+1}(\mathbf{k}) = E(\mathbf{k}) \hat{b}_l(\mathbf{k}); \\
 e^{i(k_y + 2\pi f(l + \frac{1}{3}))} \hat{a}_l(\mathbf{k}) - (e^{i(k_x + k_y + 2\pi f(l + \frac{2}{3}))} + e^{ik_x}) \hat{a}_{l+1}(\mathbf{k}) \\
 = E(\mathbf{k}) \hat{c}_l(\mathbf{k}) \quad (10)
 \end{aligned}$$

where $l = 0; 1; \dots; q-1$ is the flavor indices and $a; b; c$ are the 3 color indices.

For the simplest gauge shown in Fig.10b, we need to distinguish two general cases: $q = 3n$ and $q \neq 3n$. For $q \neq 3n$, we find out there are still two subcases: q is even and q is odd.

When q is small, we can solve the Harper's equation analytically. For $q = 1$ which is the nonmagnetic field case, there are 3 bands: $\frac{3 + 2(\cos k_x + \cos k_y + \cos(k_x - k_y))}{q}$ and 0. The lowest band is $E(k) = \frac{3 + 2(\cos k_x + \cos k_y + \cos(k_x - k_y))}{q}$. The minimum is at $(0;0)$. For $q = 2$, all the 6 bands are completely flat. The energies are $E = \frac{6}{q}; 0; \frac{6}{q}$, each with degeneracy 2. For $q = 3$, there are also 3 bands: $\frac{6 + 2A(k_x; k_y)}{q}$ and 0. The lowest band is $E(k) = \frac{6 + 2A(k_x; k_y)}{q}$ where $A(k_x; k_y) = \cos k_x + \cos k_y + \cos(k_x - k_y) + \cos(k_y + \frac{4}{3}) + \cos(k_y - k_x + \frac{2}{3}) + \cos(k_x + \frac{2}{3})$. The two minima are at $(0;0)$ and $(\frac{2}{3}; \frac{2}{3})$.

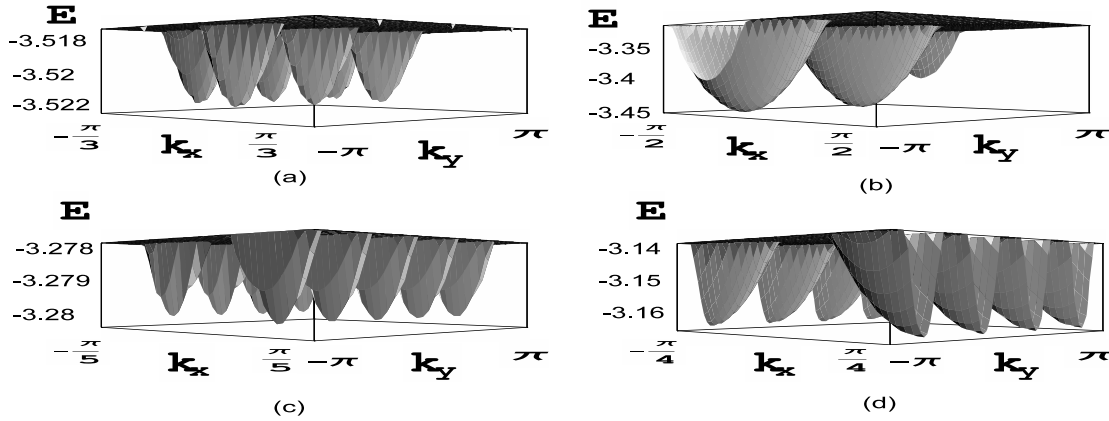


Fig 11: The lowest energy bands of dice lattice at (a) $q = 9$, (b) $q = 6$, (c) $q = 5$, (d) $q = 4$

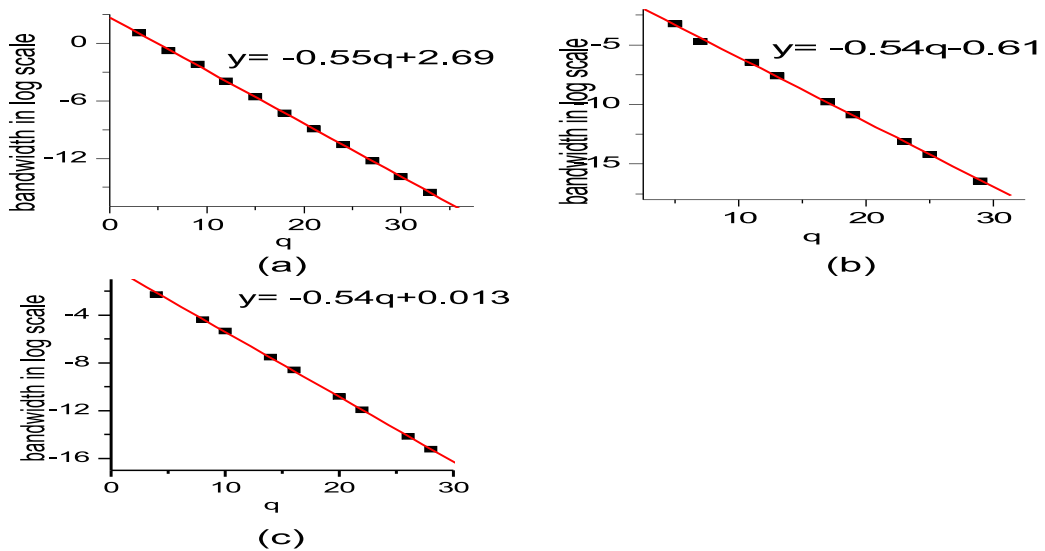


Fig 12: The bandwidths of dice lattice vs q (a) $q = 3n$, (b) $q \neq 3n$ and odd, (c) $q \neq 3n$ and even

In general, there are four cases in the dice lattice: (1) $q = 3n, \frac{3}{q} = k_x - \frac{3}{q}$. There are q bands. We also need to distinguish two subcases: (1a). n is odd, there are $2n$ minima at $(0; \frac{2}{n}-1)$ and $(\frac{2}{3n}; \frac{2}{3n} + \frac{2}{n}-1); l = 0; \dots; n-1$. $q = 9$ case is shown in Fig.11 (a).

(1b). n is even, there are n minima at $(\frac{2}{3n}; \frac{2}{3n} + \frac{2}{n}l); l=0; \dots; n-1$. $q=6$ case is shown in Fig.11 (b). For both cases, the bandwidth falls as $14.73e^{-0.55q}$ as shown in Fig.12 (a).
 (2) $q \notin 3n, \frac{2}{q} \neq \frac{k}{q}$. There $3q$ bands. We also need to distinguish two subcases:
 (2a). q is odd, there are $2q$ minima at $(\frac{2}{3q}; \frac{2}{3q} + \frac{2}{q}l) = \dots; l=0; \dots; q-1$. $q=5$ case is shown in Fig.11 (c). The bandwidth falls as $0.54e^{-0.54q}$ as shown in Fig.12 (b).
 (2b). q is even, there are q minima at $(\frac{2}{q}; \frac{2}{q} + \frac{2}{q}l); l=0; \dots; q-1$. $q=4$ case is shown in Fig.11 (d), the bandwidth falls as $1.01e^{-0.54q}$ as shown in Fig.12c.

It seems to us that all the four cases have the same exponential errors, but with different magnitudes A .

6. Kagome lattice

Kagome lattice is not a Bravais lattice either, it can be thought as a underlying parallelogram Bravais lattice with two primitive lattice vectors $\mathbf{a}_1 = \hat{x}; \mathbf{a}_2 = \frac{1}{2}\hat{x} + \frac{\sqrt{3}}{2}\hat{y}$ plus a three point basis labeled $a; b; c$ located at $\mathbf{x}; \mathbf{x} + \mathbf{a}_1; \mathbf{x} + \mathbf{a}_2$ as shown in Fig.13. Note that the Kagome lattice contains both triangles and hexagons.

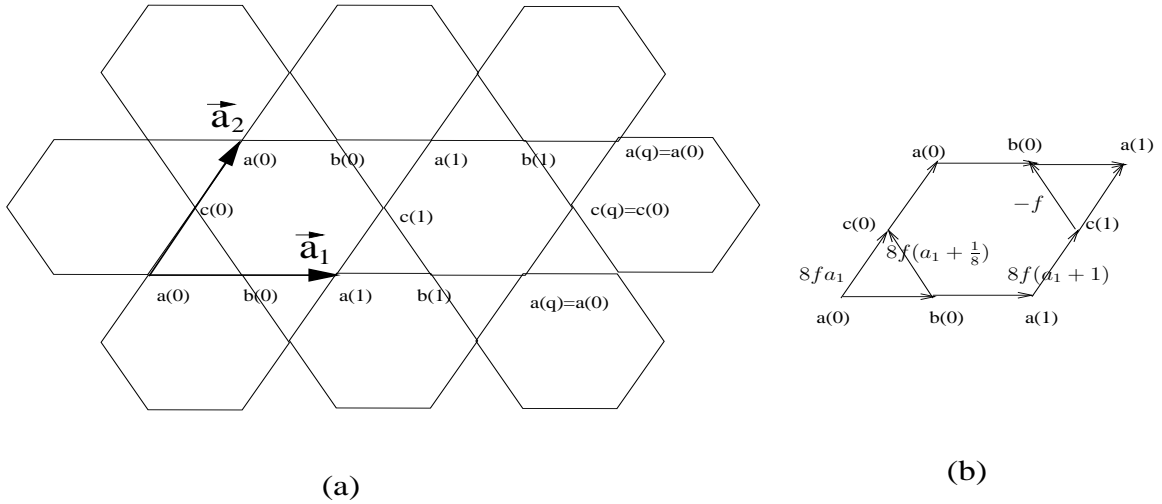


Fig 13: Kagome lattice (a) magnetic unit cell of Kagome lattice, (b) Phase factors on bonds, 0 phase factors are not shown.

We are looking at the Hofstadter band of vortices hopping around a Kagome lattice in the presence of magnetic flux $f = p/q$ per triangle and $6f$ flux quantum per hexagon. So overall, there are $8f$ flux quanta per parallelogram. For the simplest gauge chosen in Fig 13b, the Hamiltonian is:

$$\begin{aligned}
 H = & \sum_{\mathbf{x}} t \left[\left| \mathbf{j} + \frac{\mathbf{a}_1}{2} \right\rangle \langle \mathbf{x} | + \left| \mathbf{j} + \frac{\mathbf{a}_2}{2} \right\rangle \langle \mathbf{x} | e^{i2\pi 8fa_1} \left| \mathbf{j} + \frac{\mathbf{a}_1}{2} \right\rangle \langle \mathbf{x} + \frac{\mathbf{a}_1}{2} | \right. \\
 & + \left| \mathbf{j} + \frac{\mathbf{a}_2}{2} \right\rangle \langle \mathbf{x} + \frac{\mathbf{a}_2}{2} | + \left| \mathbf{j} + \frac{\mathbf{a}_1}{2} + \frac{\mathbf{a}_2}{2} \right\rangle \langle \mathbf{x} + \frac{\mathbf{a}_1}{2} + \frac{\mathbf{a}_2}{2} | e^{i2\pi f} \left| \mathbf{x} + \frac{\mathbf{a}_1}{2} + \frac{\mathbf{a}_2}{2} \right\rangle \\
 & \left. + \left| \mathbf{j} + \frac{\mathbf{a}_2}{2} \right\rangle \langle \mathbf{x} + \frac{\mathbf{a}_2}{2} | e^{i2\pi 8f(a_1 + \frac{1}{8})} \left| \mathbf{x} + \frac{\mathbf{a}_1}{2} \right\rangle \langle \mathbf{x} + \frac{\mathbf{a}_1}{2} | + \text{h.c.} \right] \quad (11)
 \end{aligned}$$

The corresponding Harper's equation is:

$$\begin{aligned}
 & \begin{pmatrix} b \\ 1 \end{pmatrix}(\mathbf{k}) = \begin{pmatrix} e^{ik_x} & b \\ 1 & 1 \end{pmatrix}(\mathbf{k}) \begin{pmatrix} e^{ik_y} + e^{i2\pi f} & c \\ 1 & 1 \end{pmatrix}(\mathbf{k}) = E(\mathbf{k}) \begin{pmatrix} a \\ 1 \end{pmatrix}(\mathbf{k}); \\
 & \begin{pmatrix} a \\ 1 \end{pmatrix}(\mathbf{k}) = \begin{pmatrix} e^{ik_x} & a \\ 1 & 1 \end{pmatrix}(\mathbf{k}) \begin{pmatrix} e^{i2\pi f(1+\frac{1}{q})} & c \\ 1 & 1 \end{pmatrix}(\mathbf{k}) \begin{pmatrix} e^{i(2\pi f + k_x - k_y)} & c \\ 1 & 1 \end{pmatrix}(\mathbf{k}) \\
 & = E(\mathbf{k}) \begin{pmatrix} b \\ 1 \end{pmatrix}(\mathbf{k}); \\
 & \begin{pmatrix} e^{ik_y} + e^{i2\pi f} & a \\ 1 & 1 \end{pmatrix}(\mathbf{k}) \begin{pmatrix} e^{i2\pi f(1+\frac{1}{q})} & b \\ 1 & 1 \end{pmatrix}(\mathbf{k}) \\
 & \begin{pmatrix} e^{i(2\pi f + k_x - k_y)} & b \\ 1 & 1 \end{pmatrix}(\mathbf{k}) = E(\mathbf{k}) \begin{pmatrix} c \\ 1 \end{pmatrix}(\mathbf{k})
 \end{aligned} \tag{12}$$

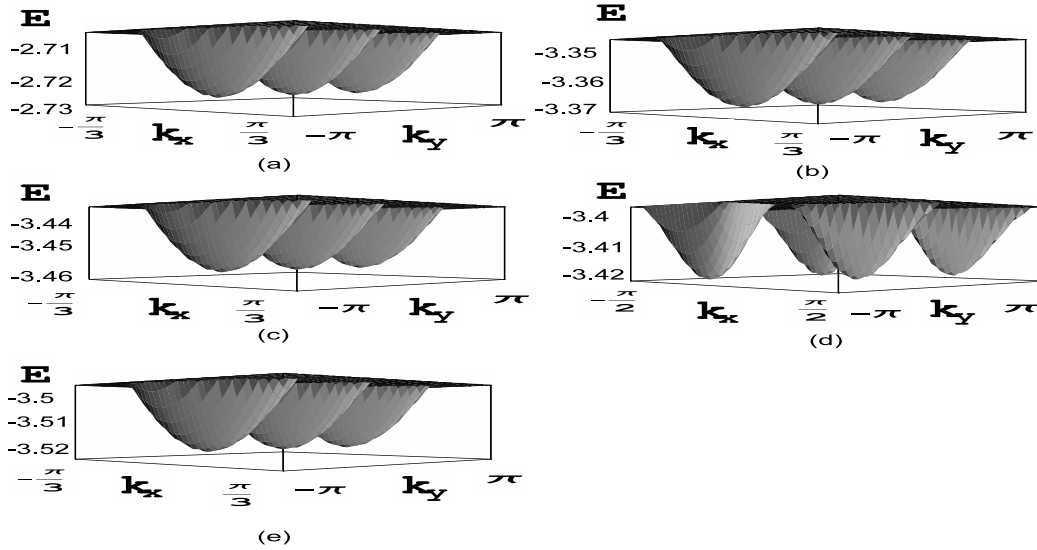


Fig 14: The lowest energy bands of Kagome lattice at (a) $q = 3$, (b) $q = 6$, (c) $q = 12$, (d) $q = 16$, (e) $q = 24$.

For the gauge chosen in Fig.13a, we can solve the spectra at $q = 1; 2; 4; 8$ exactly, because for all the four cases, we only need to solve a 3 by 3 matrix whose secular equation is a cubic equation $(4 + A(\mathbf{k}_x; \mathbf{k}_y))^3 + 2 \cos(\frac{2\pi}{q}) A(\mathbf{k}_x; \mathbf{k}_y) = 0$ where $A(\mathbf{k}_x; \mathbf{k}_y) = 2 + 2(\cos k_x + \cos k_y + \cos(k_x - k_y))$. There are 3 bands. For $q = 1$ which is the non-magnetic case, the 3 bands are $\frac{1}{q} \frac{1 + A(\mathbf{k}_x; \mathbf{k}_y)}{1 + A(\mathbf{k}_x; \mathbf{k}_y)}; 0$. The lowest band is $E(\mathbf{k}) = \frac{1}{q} \frac{1 + A(\mathbf{k}_x; \mathbf{k}_y)}{1 + A(\mathbf{k}_x; \mathbf{k}_y)}$ whose minimum is at $(0; 0)$. For $q = 2$, the 3 bands are $\frac{2}{q}; \frac{1}{q} \frac{1 + A(\mathbf{k}_x; \mathbf{k}_y)}{1 + A(\mathbf{k}_x; \mathbf{k}_y)}; \frac{1}{q} \frac{1 + A(\mathbf{k}_x; \mathbf{k}_y)}{1 + A(\mathbf{k}_x; \mathbf{k}_y)}$. We can see the lowest band is completely at, the second band touches the lowest band at $\mathbf{k} = (0; 0)$ where the gap vanishes! For $q = 4$, the 3 bands are $\frac{4}{q} + A(\mathbf{k}_x; \mathbf{k}_y); 0$. The lowest band is $E(\mathbf{k}) = \frac{4}{q} + A(\mathbf{k}_x; \mathbf{k}_y)$. The minimum is at $(0; 0)$. For $q = 8$, we need to solve the cubic equation numerically, the minimum of the lowest band is found to be at $(0; 0)$.

In general, there are 5 cases in Kagome lattice: (1) $q = n$ is odd, $\frac{1}{q} \frac{k_x}{q} - \frac{1}{q}$, there are q minima in the spectrum at $(0; \frac{2}{q}l); l = 0; 1; \dots; q-1$, $q = 3$ case is shown in Fig.14(a). We find that the bandwidth does not satisfy the exponential law as shown in Fig.15a. (2) $q = 2n$ with n odd, $\frac{2}{q} \frac{k_x}{q} - \frac{2}{q}$, there are $\frac{q}{2}$ minima at $(0; \frac{4}{q}l); l = 0; 1; \dots; \frac{q}{2}-1$, $q = 6$ case is shown in Fig.14(b). But when $q = 2$,

as shown above, the lowest energy band is completely flat. From Fig.15b, we can clearly see two separate straight lines. We divide the data into separate sets. For set 1 in Fig.15b1, the bandwidth falls as $0.33e^{-0.20q}$. For set 2 in Fig.15b2, we have the bandwidth falls as $0.10e^{-0.20q}$. (3) $q = 4n$ with n odd, $\frac{4}{q} \leq k_x \leq \frac{4}{q}$, there are $\frac{q}{4} m$ minima at $(0; \frac{8}{q}l); l = 0; \dots; q=4-1, q = 12$ is shown in Fig.14(c). The bandwidth falls as $2.46e^{-0.21q}$ as shown in Fig.15(c). (4) $q = 8n, \frac{8}{q} \leq k_x \leq \frac{8}{q}; l = 0; 1; \dots; q=8-1$, there are also two subcases (4a) when n is even, there are $2n m$ minima at $(\frac{1}{3n}; \dots + \frac{2}{3n}l)$ $= \dots$. $q = 16$ is shown in Fig.14(e). (4b) When n is odd, there are $n m$ minima at $(0; \frac{16}{q}l)$, $q = 24$ is shown in Fig.14(d). For both cases, the bandwidth falls as $13.87e^{-0.21q}$ as shown in Fig.15(d). There are $3n$ bands in all these cases.

It seems to us that all the above cases have the same c within numerical errors, but with different magnitude A .

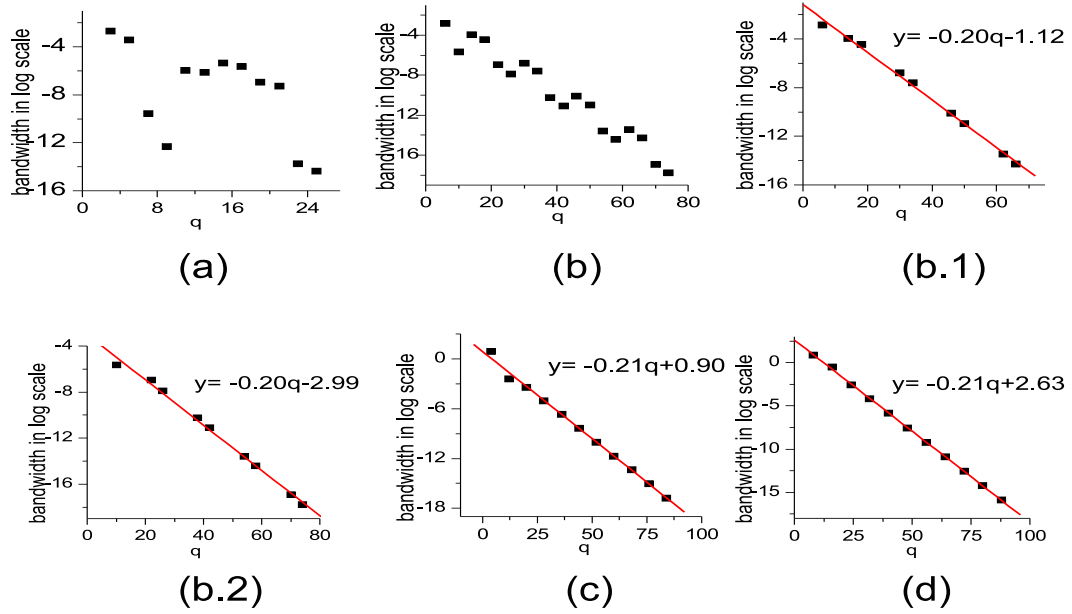


Fig 15: The bandwidth of the bands in Kagome lattice at (a) q is odd, (b) $q = 2n$ with n odd, (b.1) $q = 2n$ case 1, (b.2) $q = 2n$ case 2, (c) $q = 4n$ with n odd, (d) $q = 8n$

7. Summary and conclusions

In this paper, we have studied the energy spectra of the Hofstadter band of vortices hopping on 2D lattices in the presence of magnetic flux $\phi = \frac{p}{q}$ per smallest plaquette. Our results on dice and Kagome lattices are most new and interesting. The number of the energy bands and the number of minima in the lowest band in the 2D lattices are listed in table 1.

bipartite	square	Honeycomb	
	$N_q^n = q$	$N_q^n = \begin{matrix} 2n; & n = e \\ n; & n = o \end{matrix}$	
	q bands	$2q$ bands	
frustrated	triangular	dice	Kagome
	$N_q^{2n} = \begin{matrix} n; & n = e \\ 2n; & n = o \end{matrix}$	$N_q^{3n} = \begin{matrix} n; & n = e \\ 2n; & n = o \end{matrix}$	$N_q^n = n = o$
	$\frac{q}{2}$ bands	$3n$ bands	$N_q^{2n} = n = o$
	$N_q^o = q$	$N_{q \notin 3n}^e = q$	$N_q^{4n} = n = o$
	q bands	$N_{q \notin 3n}^o = 2q$	$N_q^{8n} = \begin{matrix} 2n; & n = e \\ n; & n = o \end{matrix}$
		above two have $3q$ bands	all cases have $3n$ bands

Table 1: The number of minimum of the lowest Hofstadter bands in the 5 lattices. N_q^n means $q = n$. S_u x e and o mean even and odd. We also list the total number of bands just below each cases. At $q = 2$, the lowest band in Kagome and dice lattices is completely flat.

It was argued in [9] that for large q , the bandwidth of the lowest energy Hofstadter band in square lattice scales as $W = A e^{-cq}$ with $c > 1$. We believe that although the argument seems reasonable, it is far from being convincing. So it is important to test this argument by quantitative numerical calculations. We tested the rule by numerically calculating the bandwidths of the lowest Hofstadter bands in the 5 lattices. We found that this rule is indeed satisfied for all the lattices even for smallest values of $q = 1$ except the Kagome lattice for q is odd. For Kagome and dice lattices, the lowest band is completely flat at $q = 2$. The results of $(A; c)$ for the five lattices are listed in the table 2:

Square	Honeycomb	Triangle	Dice	Kagome
(26.05; 1.20)	(11.82; 1.66)	(55.70; 0.83) _e	(14.73; 0.55) _{3n}	odd, not apply
		(9.21; 0.82) _o	(1.01; 0.54) _{$e \notin 3n$}	$(0.33; 0.20)_{2n,1} :$ $(0.10; 0.20)_{2n,2}$
			(0.54; 0.54) _{$o \notin 3n$}	$(2.46; 0.21)_{4n}$
				$(13.87; 0.21)_{8n}$

Table 2: The bandwidth parameters $(A; c)$ of the lowest Hofstadter bands in the 5 lattices. S_u x e (o) means q is even (odd). At $q = 2$, the lowest band in Kagome and dice lattices is completely flat.

From table 2, it is easy to see that for a given lattice, although the prefactor A could be different for different cases, the c remains the same within the numerical errors for a given lattice. For Kagome lattice when q is odd, the bandwidth does not satisfy any exponential decay law. However, in any other cases, they do satisfy the exponential laws. The peculiarity of Kagome lattice may be related to the fact that, in contrast to all the other 4 lattices, Kagome lattice has both triangles which enclose flux quanta and hexagons which enclose 6 flux quantum.

As said in the introduction, the first motivation to study the bandwidth is to look at the valid regime of dual vortex approach in the 5 lattices. If q is too large, the

bandwidth becomes too small, the dual vortex approach may not be valid anymore. For example, on square lattice, when $q = 4$, $W = 0.21$ is already very small. This fact puts some doubts on the results of CDW formations in high temperature superconductors in [9] where q as large as 8;16;32 are used. In fact, large q means very dilute boson density in the direct lattice. In this case, the superfluid is probably the only ground state anyway except there are very very exotic long range interactions in Eqn.1 which may stabilize CDW and VBS. Fortunately, the $q = 2$ (which is the smallest non-trivial case) in honeycomb lattice was applied by one of the authors to study Helium and Hydrogen adsorption problems on various substrates in [12].

The second motivation is to study the tendency for interacting bosons to form a superfluid in the 5 lattices. The bandwidth is proportional to the vortex hopping matrix element, so the smallness of bandwidth favors the localization of the vortices, therefore enhance the tendency to form a superfluid. At given q , the bandwidth W decreases in the order of Triangle, Square and Honeycomb lattice. The corresponding direct lattices are honeycomb, square and triangular lattices whose coordination numbers are 3, 4 and 6. It is known that the higher coordination, the easier for bosons to get the ordered superfluid state. The conclusions achieved in dual lattice are indeed consistent with our intuition in the direct lattice.

As shown in the table 1, when $q = 2$, the lowest bands in both Dice and Kagome lattices are flat. In dice lattice, the gap between the second flat band and the lowest flat band is $\frac{1}{6}$. However, in Kagome lattice, the gap between the second dispersive band and the lowest flat band vanishes at $\mathbf{k} = (0;0)$, so the second dispersive band can not be ignored even in the lowest energy limit. In dice lattice, all the three bands are flat, the vortices are completely inert, the interactions certainly favor the localization of the vortices. It indicates that for the original boson at half filling ($q = 2$) with nearest neighbor hopping on the Kagome lattice, there could only be a superfluid state. Slightly away from half filling, it was known that the superfluid state is stable against small number of vacancies or interstitials, we expect the superfluid state remains stable. This is in sharp contrast to bosons at half filling hopping on triangular lattice where there is a dispersion in the lowest band as shown in this paper. Due to the competition between the kinetic energy and the interactions between the vortices, there is a transition from a superfluid to a supersolid state as shown in [7]. The $q = 2$ case at square [9] and honeycomb [12] lattices were shown to have CDW or VBS to superfluid transition in Ising or easy-plane limit. Slightly away from half filling, in the CDW or VBS side, it was shown in [12] that there must be a CDW or VBS supersolid state intervening between commensurate CDW or VBS to Incommensurate CDW or VBS in Ising or easy-plane limit. Obviously, the behaviors of bosons on Kagome lattice at or near half filling ($q = 2$) are quite distinct from those in square, honey and triangular lattices.

It is important to stress that the exactly flat bands at $q = 2$ at Dice lattice are completely due to the special lattice structure of Dice lattice which localize the vortices. The dual vortex theory immediately leads to the boson superfluid state in the Kagome lattice. Of course, the bandwidth goes to zero at large q in any lattices. However, as

The mobility of dual vortices in honeycomb, square, triangular, Kagome and dice lattices is stated in previous paragraphs, the dual vortex theory is not valid anymore at sufficiently large q .

The main body of this paper only discusses the $p = 1$ case. Taking complex conjugate on the Harper's equation $H(\mathbf{k}) = E(\mathbf{k})$ leads to $H^*(\mathbf{k}) = E^*(\mathbf{k})$. Obviously, H^* corresponds to f which is equivalent to $1 - f = 1 - p = q$, so $p = 1$ has the same energy spectra as $p = q - 1$ for non-interacting vortices. Of course, vortex interactions will not have the periodicity $f \rightarrow 1 + f$ anymore, so $p = 1$ and $p = q - 1$ in Eqn.1 may not be equivalent.

In a future publication, we are trying to understand by analytical methods similar to the ones used in [20] (1) why $W = Ae^{\alpha q}$ is satisfied at even smallest value of q ? Is this a unique feature of any tight binding model? (2) For different cases on triangular and dice lattices and Kagome lattice for q is even listed in Table 2, why c is the same within the numerical errors, while A differs? (3) What is the bandwidth rule in Kagome lattice for odd q ? We will also construct MSG's for dice and Kagome lattice to understand the energy spectra structure in Table 1.

J. Ye thanks E. Fradkin for helpful discussions.

APPENDIX

In this appendix, we simply list the Harper's equations in the symmetric method first used in [9]. They may look different from those corresponding equations got by MBZ method used in the main text, but we show that both lead to the same Hofstadter bands in the 2D lattices. This check ensure the correctness of the results in the main text.

(1) Square lattice

$$e^{ik_y} \psi_{l+1} - 2 \cos(k_x + 2\pi fl) \psi_l - e^{-ik_y} \psi_{l-1} = E \psi_l \quad (A-1)$$

where $l = 0; \dots; q-1; k_x = \frac{\pi}{q}$

(2) Honeycomb lattice

$$\begin{aligned} (1 + e^{i(k_x + 2\pi fl)}) \psi_l^a - e^{ik_y} \psi_{l+1}^a &= E \psi_l^b \\ (1 + e^{i(k_x + 2\pi fl)}) \psi_l^b - e^{ik_y} \psi_{l+1}^b &= E \psi_l^a \end{aligned} \quad (A-2)$$

where $l = 0; \dots; q-1; k_x = \frac{\pi}{q}$.

(3) Triangular lattice

$$(e^{ik_y} + e^{i(k_x + k_y + 2\pi fl)}) \psi_{l+1} - (e^{ik_x} + e^{i(k_x + k_y + 2\pi fl)}) \psi_{l-1} - 2 \cos(k_x + 2\pi fl) \psi_l = E \psi_l \quad (A-3)$$

where $l = 0; \dots; q-1; k_x = \frac{\pi}{q}$ for q odd, $l = 0; \dots; q-2$ for q even.

(4) Dice lattice

$$\begin{aligned}
 (1 + e^{i(k_x + 2 - 3f)l}) \frac{a}{1} e^{ik_2} \frac{a}{1+1} &= E \frac{b}{1}; \\
 e^{i(k_x + 2 - 3f)l} \frac{a}{1} (e^{i(k_y - 2 - f)} + e^{i(k_x + k_y + 2 - 3f)(l+1) - 4 - f}) \frac{a}{1+1} &= E \frac{c}{1}; \\
 (1 + e^{i(k_x + 2 - 3f)l}) \frac{b}{1} e^{ik_y} \frac{b}{1+1} e^{i(k_x + 2 - 3f)l} \frac{c}{1} \\
 (e^{i(k_y - 2 - f)} + e^{i(k_x + k_y + 2 - 3f)(l+1) - 4 - f}) \frac{c}{1+1} &= E \frac{a}{1}
 \end{aligned} \quad (A-4)$$

where for $q \notin 3n; l = 0; \quad ; q \frac{1}{q} - 1; k_x = \frac{1}{q}$. For $q = 3n, l = 0; \quad ; q = 3$
 $1; \frac{3}{q} - k_x = \frac{3}{q}$.

(5) Kagome lattice

$$\begin{aligned}
 (1 + e^{i(k_x + 2 - 8f)l}) \frac{a}{1} e^{i2 - f} \frac{c}{1+1} e^{i(2 - f + k_y - k_x - 2 - 8f)l} \frac{c}{1} &= E \frac{b}{1}; \\
 \frac{a}{1+1} e^{i2 - f} \frac{b}{1+1} e^{ik_y} \frac{a}{1} e^{i(2 - f + k_y - k_x - 2 - 8f)l} \frac{b}{1} &= E \frac{c}{1}; \\
 (1 + e^{i(k_x + 2 - 8f)l}) \frac{b}{1} \frac{c}{1+1} e^{ik_y} \frac{c}{1} &= E \frac{a}{1}
 \end{aligned} \quad (A-5)$$

where for q is odd, $l = 0; \quad ; q \frac{1}{q} - 1; k_x = \frac{1}{q}$, for $q = 2n$ with n odd, $l = 0; \quad ; q = 2 \frac{1}{q} - 1; k_x = \frac{2}{q}$. For $4n$ with n odd, $l = 0; \quad ; q = 4 \frac{1}{q} - 1; k_x = \frac{4}{q}$. For $q = 8n, l = 0; \quad ; q = 8 \frac{1}{q} - 1; k_x = \frac{8}{q}$.

References

- [1] M. Bretz, J. G. Dash, D. C. Hickemell, E. O. McLean, and O. E. Vilches, Phys. Rev. A 8, 1589-1615 (1973).
- [2] L. W. Bush, M. W. Cole and E. Zaremba, Physics Absorption Force and Phenomena (Clarendon Press, Oxford, 1997).
- [3] K. M. O'Hara, S. L. Hemmer, M. E. Gehm, S. R. Granade, and J. E. Thomas, Science, 298, 2179 (2002).
- [4] Markus Greiner, Olaf Mandel, Tilman Esslinger, Immanuel Bloch Nature, 415, 39 - 44 (03 Jan 2002).
- [5] M. P. A. Fisher, P. B. Weichman, G. G. Rinstein and D. S. Fisher, Phys. Rev. B 40, 546 (1989).
- [6] G. C. Batrouni et al, Phys. Rev. Lett. 74, 2527 (1995).
- [7] Ganpathy Murthy, Daniel Arovas, Assa Auerbach, Phys. Rev. B 55, 3104-3121 (1997).
- [8] Jinwu Ye, Phys. Rev. B 58, 9450-9459 (1998).
- [9] L. Balents, L. Bartosch, A. Burkov, S. Sachdev, K. Sengupta, Phys. Rev. B 71, 144508 (2005).
- [10] D. R. Hofstadter, Phys. Rev. B 14, 2239-2249 (1976). J. Zak, Phys. Rev. 134, A1602-A1606 (1964), Phys. Rev. 134, A1607-A1611 (1964).
- [11] A. A. Burkov and Leon Balents, Phys. Rev. B 72, 134502 (2005).
- [12] Jinwu Ye, cond-mat/0503113.
- [13] C. Dasgupta and B. I. Halperin, Phys. Rev. Lett. 47, 1556-1560 (1981).
- [14] Horst W. Lechert and Klaus-Dieter Kortmann, Norbert Ster, Phys. Rev. B 70, 125410 (2004).
- [15] Crowell P. A. and Reppy J. D, Phys. Rev. Lett. 70, 3291C 3294 (1993)
- [16] Crowell P. A. and Reppy J. D. Phys. Rev. B 53, 2701C 2718 (1996).
- [17] Jinwu Ye, unpublished
- [18] This bandwidth is much smaller than the Landau level cyclotron gap $\omega_c = q$ in the limit of large q . In this limit, the magnetic flux through one plaquette gets very small, so one is approaching the continuum limit where the Landau levels have zero width

- [19] Recently, one of the authors applied the hard core boson Hubbard model on square lattice near half filling in the Ising limit to study the imbalanced driven quantum phase transitions in the excitonic normal solid side in the bilayer quantum Hall systems. See, Jinwu Ye, cond-mat/0407088.
- [20] D. J. Thouless, M. Kohmoto, M. P. Nightingale, and M. den Nijs, Phys. Rev. Lett. 49, 405-408 (1982).
- [21] After this paper was submitted, we learned a related and independent work by K. Sengupta, S. V. Isakov, Yong Baek Kim, cond-mat/0601175.